Orientation of capture antibodies on gold nanoparticles to improve the sensitivity of ELISA-based medical devices

Vanessa Susini [a],[*],[1], Giovanni Ferraro [b],[1], Vanna Fierabracci [a], Silvia Ursino [a], Chiara Sanguinetti [a], Laura Caponi [a], Nadia Romiti [a], Veronica Lucia Rossi [c], Antonio Sanesi [c], Aldo Paolicchi [a], Maria Franzini [a],[1], Emiliano Fratini [b],[1]

[a] *Department of Translational Research and of New Surgical and Medical Technologies, University of Pisa, Via Savi 10, Pisa, 56126, Italy*
[b] *Department of Chemistry "Ugo Schiff" & Center for Colloid and Surface Science (CSGI), University of Florence, Via Della Lastruccia 3, Sesto Fiorentino, 50019, Florence, Italy*
[c] *BioMérieux Italia S.p.a., Via di Campigliano 58, Bagno a Ripoli, 50012, Florence, Italy*

ARTICLE INFO

ABSTRACT

The sensitivity of ELISA-based devices strongly depends on the right orientation of antibodies on the sensor surface. The aim of this work was to increase the analytical performance of a commercial ELISA-based medical device (VIDAS®), thanks to the specific orientation of antibodies on gold nanostructured disposables. For this purpose, fPSA VIDAS® assay was used as model and the disposable providing the antigen binding surface (SPR®) was functionalized with gold nanostructures coated with monovalent half-fragment antibodies (reduced IgG, rIgG). The functionalization of polystyrene SPRs® with gold nanostructures was achieved through a one-step incubation of gold dispersions in a mixture of non-toxic solvents. Five different concentrations of gold nanoparticles (NPs) were tested with a maximum fluorescence enhancement for NPs density around $3–8 *10^3$ NPs/μm^2 (752 ± 11 RFV *vs* 316 ± 5 RFV of bare SPRs®). The comparison of the dose-response curve obtained with commercial and gold coated-SPRs® revealed a significant improvement ($p < 0.0001$) of the analytical sensitivity of the VIDAS® system using nanostructured disposables. This improved version of SPRs® allows to distinguish small variations of fPSA concentrations opening the way to the application of this biomarker to other kinds of cancer as recently described in the literature.

1. Introduction

Enzyme linked immunosorbent assay (ELISA) is one of the most used immunoassays and still represents the gold standard for a large number of clinical biomarkers due to its high sensitivity, specificity and throughput [1]. In recent years, ELISA technology inspired the development of medical devices, fully or partially automated, that use antibodies (Abs) as recognition element taking advantage of their high specificity for their antigens [2,3]. In the last two decades, researchers developed immunosensors that reach sensitivity at single molecule level employing complex readout mechanisms, therefore limiting their use to research studies [4–9]. VIDAS® system (bioMérieux, Marcy l'Etoile, France) is one of the most common medical device, based on ELISA technology, used in clinical laboratories. It is an automated, multiparametric immuno-analyzer for the detection of a wide panel of biomarkers for cancer, serology, cardiac diseases, and fertility. Among its advantages, VIDAS® includes fast results, easy-of-use, and reduced costs. The VIDAS® system can generate results in a time frame included between 20 min and 2 h, depending on the assay, which are shorter times than those of traditional ELISAs.

One of the main disadvantages of commercially available ELISA based devices is that capture antibodies are randomly adsorbed on hydrophobic surfaces resulting in a mixture of orientations that does not allow an efficient capture of antigens [10–12]. In VIDAS® system, capture antibodies are randomly adsorbed inside a disposable plastic tip, named Solid Phase Receptacle (SPR®), that serves as capture surface as well as pipetting system. The performances of this kind of medical device can be significantly improved by the right orientation of antibodies

---

through a proper immobilization chemistry [13–15]. In our previous work, we showed that the sensitivity of ELISA can be improved by orienting capture antibodies through the thiol groups of the hinge regions released by chemical reduction [16]. Since it is well established that free thiol groups of reduced monovalent antibody fragments (rIgG) can bind spontaneously to gold nanostructures [17–20], the aim of this work was to improve the performances of VIDAS® system functionalizing the SPRs® internal surface with gold nanostructures for the direct and controlled binding of rIgG. This approach, known as incremental innovation [21], could improve the performances of VIDAS® system maintaining its advantages and the compatibility with all the commercially available assays. Since the improvement for the free Prostate Specific Antigen (fPSA) quantification was already shown in oriented ELISA [16], the same model was used for this study to compare the performances of gold nanostructured SPRs® with the commercial assay.

2. Materials and methods

2.1. Chemicals and materials

Gold (III) chloride trihydrate ($\geq$99.9%), sodium citrate dihydrate ($\geq$99.9%) and ethanol (99%) were purchased from Sigma-Aldrich. The concentration of gold NPs dispersions was adjusted using a diafiltration cell (Millipore, 50 ml) equipped with an ultrafiltration membrane (Millipore YM10, NMWL 10000, regenerated cellulose). All the bare SPRs® disposables were provided by bioMérieux Italia (Bagno a Ripoli, Italia) and are producedmade using a commercial polystyrene-based polymer.

Mouse monoclonal anti-free prostate specific antigen (anti-fPSA) antibody and VIDAS® fPSA assay ref. 30,440 were supplied by bioMérieux Italia (Bagno a Ripoli, Italia). Sephadex G-25 in PD-10 desalting columns (GE Healthcare, Little Chalfont, UK), 2-Mercaptoethylamine (2-MEA), ethylenediaminetetraacetic acid disodium salt (EDTA), Coomassie Brillant Blue R-250, Ca^{2+} and Mg^{2+} free Dulbecco's Phosphate Buffered Saline (PBS), fat free milk and Tween-20 were purchased from Sigma Chemical Co. (St. Louis, MO, USA). Deionized water purified by a Millipore Milli-Q gradient system (>18 MΩ cm) was used in all the experiments.

3. VIDAS® fPSA assay

In VIDAS® fPSA assay, the pipetting system is constituted by the disposable SPRs® that are internally coated by non-specific adsorption of capture monoclonal anti-fPSA antibody. Washing solutions, detection anti-fPSA antibody conjugated with alkaline phosphatase, and fluorescent substrate are contained in a 10-wells disposable strip. The quantification of immunocomplexes is achieved by the hydrolysis of 4-methylumbelliferyl phosphate (4-MUP) to 4-methylumbelliferone (4-MU) by alkaline phosphatase. The fluorescent signal generated by the hydrolyzed 4-MU is proportional to the concentration of analyte in the sample and it is assessed by a single channel fluorometer [22]. Fluorescence is expressed in Relative Fluorescence Value (RFV) that is the difference between the final and the background fluorescent readings. The kit also includes the calibrator S1 (fPSA 6.9 ng/ml), the positive control C1 and the sample diluent (VIDAS® assay package insert 09573 F, version of 2006/12).

4. Preparation and characterization of gold-functionalized SPRs®

The procedure for the decoration of commercial SPRs® with gold nanoparticles was optimized in this work. Briefly, citrate-capped gold NPs were prepared using citrate as stabilizing and reducing agent (gold/citrate molar ratio: 0.13) [23]. Following this protocol, gold NPs of about 10 $\pm$ 2 nm in diameter with a negative zeta potential (around −30 mV) were obtained (see data in Supplementary Information file SI,

Fig. S1). The concentration of the aqueous gold dispersions was adjusted using a diafiltration cell to reduce the volume of the starting dispersion up to 80% and aliquots of gold NPs dispersions at different concentrations were used for the adhesion step inside the SPRs® disposables. The adhesion of gold NPs to the plastic surface of the SPRs® was performed incubating the gold dispersions in the sealed SPRs® in the presence of a certain amount of organic polar solvent (i.e. ethanol) which promotes the migration of NPs from the solution to the surface. All the coated SPRs® disposables were prepared at room temperature with 24 h of incubation time. Using this approach, all gold NPs migrate from the bulk solution to the plastic surface as demonstrated by the absence of the characteristic plasmon absorption peak of gold NPs in the visible spectra acquired on the incubated dispersion at the end of the procedure (see spectra in SI file, Fig. S2). Five different gold functionalized SPRs® (gold-SPRs®) were prepared using dispersions at different concentration to obtain plastic loading around 0.6, 1.3, 2.6, 7.9 and 15.9 $\ast 10^3$ NPs/μm^2. These values were estimated considering the exposed inner surface of the SPRs® and the concentration of gold NPs in the starting dispersions.

It is worth noting that the values of NPs density are slightly overestimated at the meniscus since a local solvent evaporation at water/air interface might concentrate NPs in the upper part of the disposable. Nevertheless, this does not affect the performances of SPRs® during the assay since the underlying SPRs® surface is homogeneously coated by gold nanoparticles.

All the gold-decorated SPRs® were characterized through scanning electron microscopy (SEM). SEM micrographs were acquired using a high-resolution scanning electron microscope (ΣIGMA, Carl Zeiss) based on the GEMINI column, which features a high brightness Schottky field emission source, beam booster, in-lens and Everhart–Thornley (ET) secondary electron detectors. The micrographs were acquired with the in-lens detector exposing to the electronic beam 0.5 cm $\times$ 0.5 cm portions of the inner surface of gold coated SPRs® disposables with an acceleration potential of 2 kV and a working distance of about 3 mm. When using the ET detector, an accelerating potential of 10 kV and a working distance of about 6 mm were used.

The surface coverage, fractality and lacunarity of SEM micrographs were calculated on the binary images using ImageJ (v. 1.53. t) [24] and the FracLac plug-in (Karperien, 2013). Fractality values take into account the 2D dimensionality of the gold aggregates while the lacunarity descriptor [25] helps in the evaluation of their spatial organization. Lacunarity (Λ) is calculated considering the variation of pixel density in an image using a grid with a certain size and is defined as:

$$\Lambda = \frac{\sum\limits_{g} \lambda_{\varepsilon,g}}{N_g} = \frac{\sum\limits_{g} \left(\frac{\sigma}{\mu}\right)^2_{\varepsilon,g}}{N_g} \tag{1}$$

where *g* is the orientation of the grid with respect to the image, μ is the average of pixels per cell at each *g*, ε is the size of the grid (in our case, 10 $\times$ 10 pixels) and σ is the standard deviation. Λ can be obtained summing the lacunarity obtained for a single grid orientation ($\lambda_{\varepsilon,g}$) divided by the number of orientations (N_g) used for the calculation (in our case, *g*: 12). An example of the grid used for the calculation of lacunarity on our samples is reported in Fig. S3 (see SI file).

5. Anti-fPSA antibody reduction and coating of gold-SPRs

rIgG were obtained by chemical reduction according to the previously described protocol [16]. Briefly, 1 mg/ml anti-fPSA antibodies were reduced by 53 mM 2-mercaptoethylamine (2-MEA) in PBS with 10 mM EDTA. The reduction mixture was incubated at 37 °C for 90 min under mild agitation. Then, the reducing agent and EDTA were removed using a Sephadex G-25 in PD-10 desalting column following the instruction of the manufacturer. The presence of monovalent anti-fPSA (anti-fPSA$_{red}$;75 kDa) was assessed by non-reducing 8% sodium

dodecyl sulphate polyacrylamide gel electrophoresis (SDS-PAGE); protein bands were stained with Coomassie brilliant blue R-250.

Gold-SPRs® were coated incubating 300 µl of 15 µg/ml anti-fPSA$_{red}$ [19,26] in PBS for 15 min at 37 °C on board of VIDAS®. In this case, the coating of anti-fPSA$_{red}$ on gold-SPRs® (anti-fPSA$_{red}$@gold-SPRs®) is guided by the thiol–gold chemistry allowing the fine control of the antibody orientation on the plastic surface.

Non-specific binding was blocked by 60 min incubation at 37 °C with 5% (w/v) fat free milk diluted in PBS-Tween 0.01% (v/v). The coating of gold-SPR® was performed daily.

6. Testing of anti-fPSA$_{red}$@gold-SPRs®

Twelve replicates were prepared for each kind of gold-SPRs® (0.6, 1.3, 2.6, 7.9 and 15.9 *10^3 NPs/µm^2) coated with anti-fPSA$_{red}$ antibody and tested using the VIDAS® fPSA assay kit. Calibrator S1 of VIDAS® fPSA assay diluted 1:10 in PBS (0.69 ng/ml; 316 ± 5 RFV) was used as sample. Among the tested anti-fPSA$_{red}$@gold-SPRs®, the most performing one was chosen for the subsequent comparative test with standard SPRs®. For this purpose, five concentrations of calibrator S1 diluted in PBS (i.e. 6.90 ng/ml, 3.45 ng/ml, 1.38 ng/ml, 0.14 ng/ml, and 0 ng/ml) were used as samples and each concentration was repeated twelve-fold both on standard SPRs® and anti-fPSA$_{red}$@gold-SPRs®.

7. Evaluation of the analytical performances

The analytical sensitivity and the limit of detection (LoD) of VIDAS® fPSA assay performed on anti-fPSA$_{red}$@gold-SPRs® were calculated from a calibration curve of five fPSA concentrations (i.e. 0.63 ng/ml; 0.32 ng/ml; 0.06 ng/ml; 0.02 ng/ml; 0.01 ng/ml) obtained by dilution of calibrator S1. The whole calibration curve was run in 7 consecutive days obtaining a total of 14 repetitions for each concentration. A new batch of anti-fPSA$_{red}$@gold$_D$-SPRs® was prepared every day.

The analytical sensitivity of an assay is the ability of a method to assess small variations of the concentration of analyte, and it is expressed by the slope of calibration curves [27]. LoD is the lowest analyte concentration likely to be detectable. In this study LoD values were estimated using the approach based on standard deviation of the response and the slope. This method was chosen since it allowed the estimation of LoD, sensitivity and fPSA concentrations from the same experimental data of the calibration curve. LoD values were calculated according to the formula LoD = 3.3 SD$_y$/slope (SD$_y$, standard deviation of y intercept) [28,29].

8. Tests on biological samples

Human samples used in this study were obtained from University Hospital of Pisa and were "waste of the sample examined". Privacy was maintained by the impossibility of tracing the patient's identity and, therefore, any further information.

The samples were assessed twice on commercial SPRs® and anti-fPSA$_{red}$@gold-SPRs® using the VIDAS® fPSA assay. fPSA concentrations were calculated from the experimental calibration curve when using anti-fPSA$_{red}$@gold-SPRs® or the calibration master curve of the kit for commercial SPRs®. In fact, for the commercial SPRs® the master curve of the assay is embedded in the VIDAS® system and it is tuned on the lot of the kit using the corresponding calibrator. Concerning the assay performed with anti-fPSA$_{red}$@gold$_D$-SPRs® we use as calibration curve the dose-response curve obtained from the LoD calculation.

9. Statistical analysis

Data are presented as means ± standard deviation or means and coefficient of variation (CV) as appropriate. Linear regression analysis was used to investigate the relationship between the RFV and fPSA concentrations. The slopes of the calibration curves of VIDAS® fPSA assay performed on gold nanostructured SPRs® or commercial SPRs® were compared with the F-test based on the distribution of Fisher-Snedecor at a confidence level of 95%.

All data were analyzed using GraphPad Prism v. 9.0 (GraphPad Software Inc., La Jolla, USA).

10. Results & discussion

10.1. Analytical response of anti-fPSA$_{red}$@gold-SPRs®

The response of anti-fPSA$_{red}$@gold-SPRs® prepared using different concentrations of NPs (0.6, 1.3, 2.6, 7.9 and 15.9 *10^3 NPs/µm^2) was evaluated against 0.69 ng/ml fPSA to identify the most performing system. Fig. 1 shows the coverage of the plastic surface of the SPRs® by gold NPs as a function of gold NPs density together with the corresponding SPRs®.

SEM micrographs in Fig. 1 reveal that gold NPs tend to aggregate in 3D structures before completely covering the plastic surface as the concentration of the starting dispersion is increased. The 3D growth of gold nanostructures is well visible in Fig. 1C–a, where an ET detector was used to stress the 3D morphology of the coating. Even for the highest gold NPs concentration (NPs density = 15.9 *10^3 NPs/µm^2), the full coverage of the plastic substrate could not be achieved because of the formation of a 3D porous layer with an average thickness of about 20–30 gold NPs.

Fig. 2A shows the fluorescence signal enhancement induced by the addition of the gold coating and the right antibody orientation. In the same plot the variation of coverage of the plastic surface is also reported. The RFV measured using commercial VIDAS® SPRs® when testing 0.69 ng/ml fPSA was 316 ± 5 RFV while anti-fPSA$_{red}$@gold-SPRs® produced higher RFV when the relative amount of plastic surface covered by the gold nanostructures increase. The maximum signal improvement was observed using disposables with NPs density at about 8 *10^3 NPs/µm^2 where a plateau is reached in the amount of plastic surface covered by gold nanoparticles (Fig. 1D). Increasing the amount of NPs up to 15.9 *10^3 NPs/µm^2, a definite and unexpected reduction of RFV is observed. This behavior could be ascribed to a change in the morphology of the gold layer from an open to a porous gold coating as shown in Fig. 1E. The morphology of the gold coating can be analytically described by using two geometrical descriptors, i.e., the lacunarity, Λ, and fractality, D_F [25], of the surface (see Fig. 2B). Λ is inversely proportional to the agglomeration of gold NPs on the surface while D_F accounts for the compactness of the gold layer. Λ shows a marked decrease starting from gold density of about 3 NPs/µm^2 as a result of the lower gappiness of the nanostructures assembling on the plastic surface; in parallel, D_F increases indicating the formation of gold aggregated deposits. A more compact gold layer is then responsible for an increase of the surface available for the binding of well oriented monovalent antibodies and, therefore, explains the observed fluorescence enhancement. Increasing the concentration of nanoparticles deposited per unit area, the response is not linear levelling off at 8 *10^3 NPs/µm^2 and a drop in the fluorescence signal was observed when the NPs density reaches 15.9 *10^3 NPs/µm^2. This behavior is linked to the formation of a porous 3D gold layer (see Fig. 1E) which internalizes most of the monovalent antibodies making the antigen binding sites unavailable. This effect was further confirmed by the fractality and lacunarity values found for sample E showing the presence of a "closed" ($D_F \sim 2$) and rather compact ($\Lambda \sim 0$) gold structure.

Among the investigated gold-SPRs®, sample D (referred as "gold$_D$-SPR®"; 8 *10^3 NPs/µm^2) generated the highest fluorescent signal with the lowest standard deviation (752 ± 11 RFV) and thus it was selected as the best performing candidate for the subsequent experiments.

The response of anti-fPSA$_{red}$@gold$_D$-SPRs® was compared to commercial SPRs® testing five fPSA concentrations with the VIDAS® fPSA assay (see Table 1).

For all the tested fPSA concentrations, the fluorescence signal
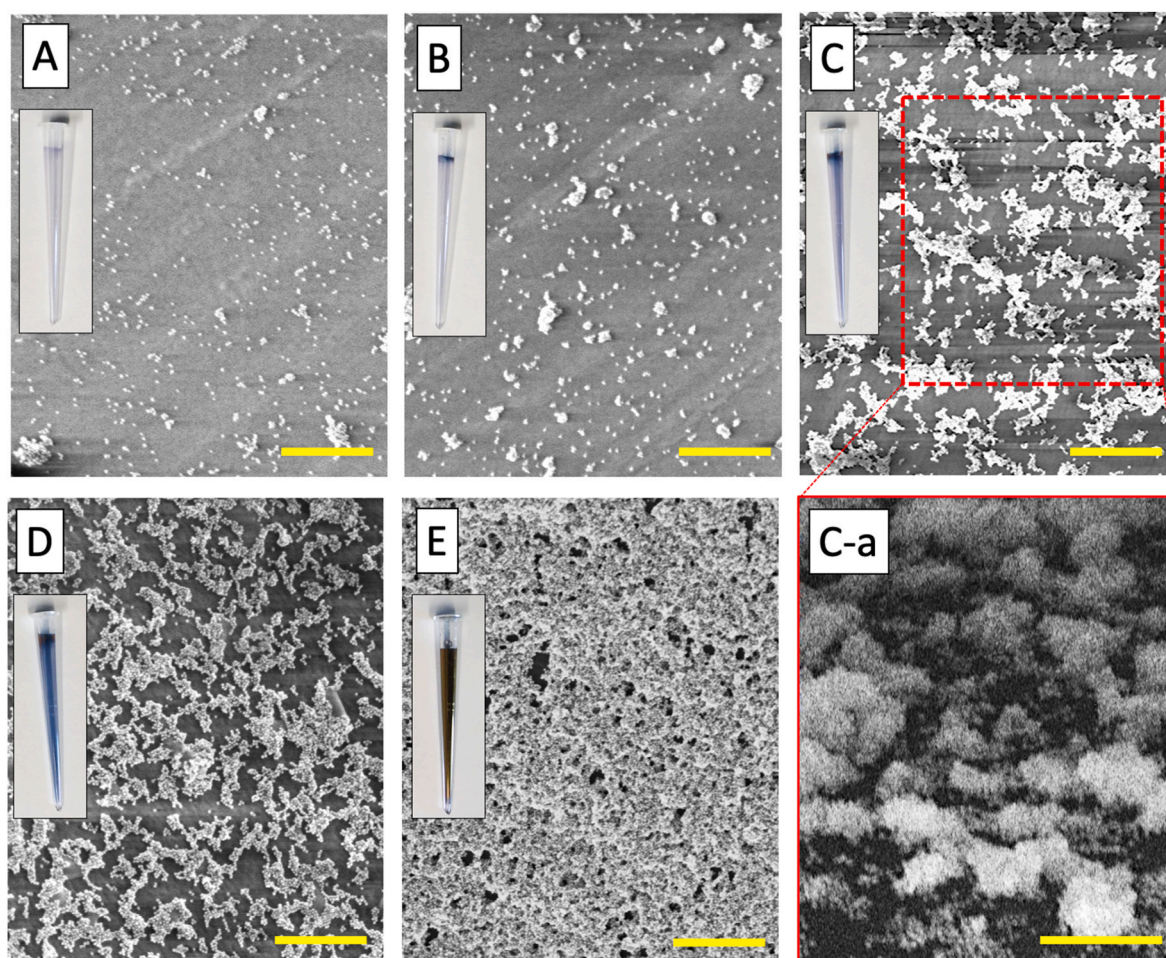
Fig. 1. SEM micrographs at the same magnification (100 kX) of the different gold-SPRs® obtained using different amounts of gold NPs: 0.6 (A), 1.3 (B), 2.6 (C), 7.9 (D) and 15.9 (E) $*10^3$ NPs/μm^2 (scale bar: 400 nm). Insets: pictures of gold-SPRs® after functionalization with NPs. Panel C–a: sample C acquired using classical the ET detector (magnification 150 kX, scale bar 200 nm).
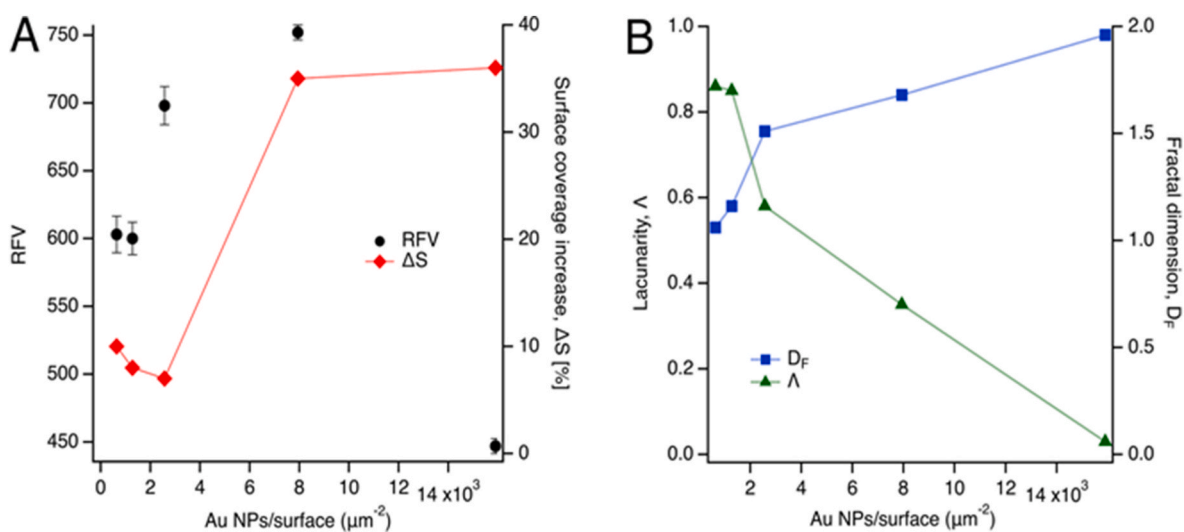
Fig. 2. Panel A: RFV values (black dots) measured using VIDAS® fPSA assay on anti-fPSA$_{red}$@gold-SPRs® together with the increment of surface coverage (ΔS) at the different gold NPs concentrations (red dots) (reference value of commercial SPRs®: 316 ± 5 RFV). Panel B: fractality, D_F, (blue dots) and lacunarity, Λ, (green dots) of the 2D NPs arrangements at different gold NPs concentrations.

Table 1

Mean fluorescence signal (n = 12) and coefficient of variation (CV) obtained using anti-fPSA$_{red}$@gold$_D$-SPRs® or commercial SPR® and reagents strips of the VIDAS® fPSA assay.

fPSA (ng/ml)	anti-fPSA$_{red}$@gold$_D$-SPRs®		Commercial SPR®	
	RFV	CV%	RFV	CV%
0	5.3	33	1.5	78
0.14	146	3	61	3
1.38	1429	2	582	2
3.45	2620	2	1688	2
6.90	5609	2	3449	3

generated by anti-fPSA$_{red}$@gold$_D$-SPRs® was roughly 2-fold higher than the one obtained with commercial SPRs® functionalized with randomly adsorbed antibodies. Furthermore, the intra-assay CV obtained with anti-fPSA$_{red}$@gold$_D$-SPRs® was comparable with that of the commercial assay, despite the in-house coting. This confirms the robustness of the techniques used to produce the anti-fPSA$_{red}$@gold$_D$-SPRs® and their potential for scalability for industrial manufacturing. The coating of gold$_D$-SPRs® with whole anti-fPSA Abs did not generate any signal enhancement confirming that the signal improvement was due to the proper orientation of reduced anti-fPSA Abs on gold NPs (Table S1 in SI file).

Finally, also the background noise of anti-fPSA$_{red}$@gold$_D$-SPRs® was comparable to that of commercial SPRs®. These results suggested that anti-fPSA$_{red}$@gold$_D$-SPRs® improve the analytical performances of fPSA assay.

11. Analytical performances: LoD and analytical sensitivity

The analytical performances of anti-fPSA$_{red}$@gold$_D$-SPRs® were further investigate using the VIDAS® fPSA assay from a calibration curve obtained testing five fPSA concentrations and using the VIDAS® fPSA diluent as blank. VIDAS® fPSA assay on commercial SPRs® was run in parallel (Table 2 and Fig. 3). The five fPSA concentrations were chosen since the detection limit reported on the package insert of VIDAS® fPSA assay (i.e., 0.05 ng/ml).

For each fPSA concentration, higher RFV values were observed using anti-fPSA$_{red}$@gold$_D$-SPRs® in comparison with the commercial ones. Linear correlation analysis of these calibration curves allowed to estimate the LoD values and the analytical sensitivity for the two SPRs types (Table 2). The calculated LoD values were in the same order of magnitude, even if lower for the commercial SPRs®. This difference was due to the higher standard deviation of y intercept value obtained with anti-

Table 2

Mean fluorescent signal (n = 14) and coefficient of variation (CV) obtained using anti-fPSA$_{red}$@gold$_D$-SPRs® or commercial SPR® and reagents strips of the VIDAS® fPSA assay.

fPSA (ng/ml)	anti-fPSA$_{red}$@gold$_D$-SPRs®		Commercial SPR®	
	RFV	CV%	RFV	CV%
0	1.5	62.7	2.4	35.7
0.013	11	10.7	4	33.0
0.025	20	4.5	7	11.0
0.063	51	9.1	26	7.2
0.317	257	6.4	138	3.1
0.634	524	5.9	279	3.6
Analytical sensitivity; 95%CI (RFV•ml/ng)	823.6; 807.2–840.1		441.2; 436.4–445.9	
SDy (RFV)	10.35		2.69	
LoD (ng/ml); 95%CI (ng/ml)	0.0415; 0.0406–0.0423		0.0201; 0.0199–0.0204	

The analytical sensitivities are expressed as the slopes of the calibration curves. SDy: standard deviation of y intercept value. LoD = 3.3 SDy/slope.
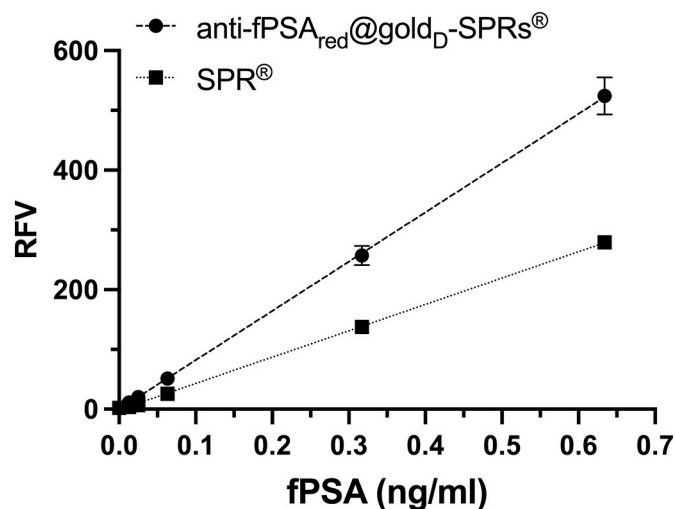
Fig. 3. Calibration curve of VIDAS® fPSA assay performed on anti-fPSA$_{red}$@gold$_D$-SPRs® (circle) or commercial SPRs®(square). Data are reported as mean ± SD (n = 14).

fPSA$_{red}$@gold$_D$-SPRs® (Table 2) which could be related to the daily in-house coating of gold$_D$-SPRs® with anti-fPSA$_{red}$. In VIDAS® system 20 RFV is the minimum detectable signal which is significantly different from the blank (technical data). It is interesting to observe that this criterion was satisfied for a lower concentration by the anti-fPSA$_{red}$@gold$_D$-SPRs® in comparison with the commercial SPRs® and the calculated LoD value (Table 2). This technical cut off value was reached with 0.025 ng/ml fPSA when using anti-fPSA$_{red}$@gold$_D$-SPRs® but only with 0.063 ng/ml with the commercial SPRs®. This result suggests that the sensitivity of VIDAS® fPSA assay performed on the anti-fPSA$_{red}$@gold$_D$-SPRs® was improved.

The anti-fPSA$_{red}$@gold$_D$-SPR® disposables also allowed a significant improvement of the analytical sensitivity in comparison to the commercial kit (p < 0.0001), it does it means that fPSA$_{red}$@gold$_D$-SPR® allows to appreciate smaller variations of analyte concentrations.

The overall results suggested that samples with concentration of fPSA in the low range (<0.2 ng/ml) can be reliably measured using anti-fPSA$_{red}$@gold$_D$-SPRs® and this could be particularly useful for the follow-up of prostatectomized patients where variations of PSA in the low range are clinically meaningful [30,31].

12. Tests on biological samples

The response of anti-fPSA$_{red}$@gold$_D$-SPRs® on biological samples was assessed running VIDAS® fPSA assay on five human plasma samples; the same was done in parallel using commercial SPRs®. Collected data (see Table 3) confirmed that higher RFV values were measured using anti-fPSA$_{red}$@gold$_D$-SPRs®.

Table 3

FPSA quantification on five human plasma samples using the anti-fPSA$_{red}$@gold$_D$-SPRs® or the commercial SPRs®.

Sample	anti-fPSAred@goldD-SPRs®		Commercial SPRs®	
	fPSA[a] (ng/ml)	RFV	fPSA[b] (ng/ml)	RFV
1	0.17	145	0.18	61
2	0.30	228	0.28	108
3	0.32	273	0.33	115
4	1.18	946	1.15	456
5	1.47	1280	1.55	581

[a] Concentrations were calculated using the calibration curve obtained from LoD calculation.

[b] Concentrations were calculated by the VIDAS® user software using the calibration master curve of the assay.

The use of the appropriate dose-response curve allowed the calculation of fPSA concentration for each sample which agreed independently of the used SPRs®, thus suggesting that plasma matrix does not interfere with the rIgG and/or the gold nanostructures on SPRs®.

The results obtained on samples 2 and 3 well exemplify the improved analytical sensitivity of the assay performed with the nanostructured disposable: indeed, the two samples showed similar fPSA concentrations which were detected with a difference of 45 RFV using anti-fPSA$_{red}$@gold$_D$-SPRs®, while only 7 RFV of difference between the two samples were measured using commercial SPRs®.

13. Conclusions

Our results showed that the implementation of oriented antibodies in a commercial VIDAS® assay improves the analytical sensitivity of the system preserving all the current advantages and its compatibility with the existing assays. In literature a new ELISA or ELISA-based device developed in house by the authors are often described. Instead, in this work an incremental innovation approach is described that allow the increase of the sensitivity of a commercial IVD labeled medical device. Unlike radical innovation, the incremental innovation approach has the advantage to increase the performance of a medical device while maintaining the compatibility with the existing analytical system and the production processes. Furthermore, the methodological approach here reported can be virtually applied to other commercialized ELISAs or ELISA-based medical devices that use polystyrene as capturing surface.

In this work, the plastic disposables of VIDAS® system (SPRs®) were directly decorated with gold nanoparticles and then functionalized with monovalent anti-fPSA antibodies resulting in a quick, simple, and scalable process. In fact, the deposition of gold NPs on polystyrene, the chemical reduction of the Abs and their coating on the gold surface require neither complex laboratory instrumentation nor the use of solvents potentially harmful to human health. The disposables here described were used with the VIDAS® fPSA assay for the detection of fPSA in plasma samples. Anti-fPSA$_{red}$@gold$_D$-SPRs® significantly increase the analytical sensitivity of the assay (p < 0.0001) in comparison to the commercial SPRs® allowing for the detection of smaller variations of analyte concentrations. Indeed, two samples with similar fPSA concentrations were detected with a difference of 45 RFV and 7 RFV using anti-fPSA$_{red}$@gold$_D$-SPRs® and commercial SPRs®, respectively. Furthermore, anti-fPSA$_{red}$@gold$_D$-SPRs® was able to quantify a lower fPSA concentration (0.025 ng/ml) than the commercial SPRs®.

The main limitation of the proposed approach is represented by the need of the daily coating of gold-SPRs® with monovalent anti-fPSA fragments. Indeed, during storage, the adsorbed antibodies could undergo tertiary structure rearrangements due to the loss of solvation shell, thus losing their antigen binding capability. Future studies will be performed to address this point and ensure the long-term stability of the SPRs® disposables required for industrialization.

It is known that PSA is produced extraprostatically in males and even in females where PSA is mainly expressed in hormonally regulated tissues [32]. The serological concentration in females in 1000-fold lower than in males [33], but, interestingly, it seems that this value increase in presence of breast tumors [34–36] suggesting a possible role of fPSA as breast cancer biomarker. In future, the developed anti-fPSA$_{red}$@gold$_D$-SPRs® will be applied in clinical studies to verify if this assay could be extended to the follow-up of prostatectomized and of breast cancer patients extending the clinical application of the current VIDAS® fPSA assay.

Credit author statement

Vanessa Susini: Conceptualization, Investigation, Writing – original draft. **Giovanni Ferraro**: Conceptualization, Investigation, Writing – original draft. **Vanna Fierabracci**: Funding acquisition. **Silvia Ursino**: Validation. **Chiara Sanguinetti**: Writing – review & editing **Laura Caponi**: Writing – review & editing. **Nadia Romiti**: Investigation. **Veronica Lucia Rossi**: Data curation, Resources. **Antonio Sanesi**: Supervision. **Aldo Paolicchi**: Project administration. **Maria Franzini**: Conceptualization, Formal analysis, Visualization, Writing – review & editing. **Emiliano Fratini**: Conceptualization, Project administration, Writing – original draft, Writing – review & editing.

Declaration of competing interest

The authors declare that they have no known competing financial interests or personal relationships that could have appeared to influence the work reported in this paper.

Data availability

I have shared the data at the attach files step

Acknowledgments

Appendix A. Supplementary data

Supplementary data to this article can be found online at https://doi.org/10.1016/j.talanta.2023.124650.

References

[1] S.K. Vashist, J.H.T. Luong, Chapter 1 - immunoassays: an overview, in: S.K. Vashist, J.H.T. Luong (Eds.), Handb. Immunoass. Technol., Academic Press, 2018, pp. 1–18, https://doi.org/10.1016/B978-0-12-811762-0.00001-3.

[2] J.D. Newman, P.J. Warner, A.P.F. Turner, L.J. Tigwell, Biosensors: a Clearer View, Cranfield University Publication, 2004. https://www.scienceopen.com/document?vid=3d793d99-9687-43b4-80e2-8d6102ecd510. (Accessed 20 July 2022).

[3] D.R. Thévenot, K. Toth, R.A. Durst, G.S. Wilson, Electrochemical biosensors: recommended definitions and classification, Biosens. Bioelectron. 16 (2001) 121–131, https://doi.org/10.1016/s0956-5663(01)00115-4.

[4] B. Gil Rosa, O.E. Akingbade, X. Guo, L. Gonzalez-Macia, M.A. Crone, L.P. Cameron, P. Freemont, K.-L. Choy, F. Güder, E. Yeatman, D.J. Sharp, B. Li, Multiplexed immunosensors for point-of-care diagnostic applications, Biosens. Bioelectron. (2022), 114050, https://doi.org/10.1016/j.bios.2022.114050.

[5] B. Liu, D. Zhang, H. Ni, D. Wang, L. Jiang, D. Fu, X. Han, C. Zhang, H. Chen, Z. Gu, X. Zhao, Multiplex analysis on a single porous hydrogel bead with encoded SERS nanotags, ACS Appl. Mater. Interfaces 10 (2018) 21–26, https://doi.org/10.1021/acsami.7b14942.

[6] I. Petrova, V. Konopsky, I. Nabiev, A. Sukhanova, Label-free flow multiplex biosensing via photonic crystal surface mode detection, Sci. Rep. 9 (2019) 8745, https://doi.org/10.1038/s41598-019-45166-3.

[7] E.A. Phillips, A.K. Young, N. Albarran, J. Butler, K. Lujan, K. Hamad-Schifferli, J. Gomez-Marquez, Ampli: a construction set for paperfluidic systems, Adv. Healthc. Mater. 7 (2018) e1800104, https://doi.org/10.1002/adhm.201800104.

[8] Y. Wan, Y. Su, X. Zhu, G. Liu, C. Fan, Development of electrochemical immunosensors towards point of care diagnostics, Biosens. Bioelectron. 47 (2013) 1–11, https://doi.org/10.1016/j.bios.2013.02.045.

[9] D.H. Wilson, D.M. Rissin, C.W. Kan, D.R. Fournier, T. Piech, T.G. Campbell, R. E. Meyer, M.W. Fishburn, C. Cabrera, P.P. Patel, E. Frew, Y. Chen, L. Chang, E. P. Ferrell, V. von Einem, W. McGuigan, M. Reinhardt, H. Sayer, C. Vielsack, D. C. Duffy, The simoa HD-1 analyzer: a novel fully automated digital immunoassay analyzer with single-molecule sensitivity and multiplexing, J. Lab. Autom. 21 (2016) 533–547, https://doi.org/10.1177/2211068215589580.

[10] J.E. Butler, Solid supports in enzyme-linked immunosorbent assay and other solid-phase immunoassays, Methods 22 (2000) 4–23, https://doi.org/10.1006/meth.2000.1031.

[11] J.E. Butler, L. Ni, R. Nessler, K.S. Joshi, M. Suter, B. Rosenberg, J. Chang, W. R. Brown, L.A. Cantarero, The physical and functional behavior of capture antibodies adsorbed on polystyrene, J. Immunol. Methods 150 (1992) 77–90, https://doi.org/10.1016/0022-1759(92)90066-3.

[12] M.E. Wiseman, C.W. Frank, Antibody adsorption and orientation on hydrophobic surfaces, Langmuir ACS J. Surf. Colloids. 28 (2012) 1765–1774, https://doi.org/10.1021/la203095p.

[13] T. García-Maceira, F.I. García-Maceira, J.A. González-Reyes, E. Paz-Rojas, Highly enhanced ELISA sensitivity using acetylated chitosan surfaces, BMC Biotechnol. 20 (2020) 41, https://doi.org/10.1186/s12896-020-00640-z.

[14] Front matter, in: D. Wild (Ed.), Immunoass. Handb., fourth ed., Elsevier, Oxford, 2013, p. iii, https://doi.org/10.1016/B978-0-08-097037-0.01001-0.

[15] L.S. Wong, F. Khan, J. Micklefield, Selective covalent protein immobilization: strategies and applications, Chem. Rev. 109 (2009) 4025–4053, https://doi.org/10.1021/cr8004668.

[16] V. Susini, L. Caponi, V.L. Rossi, A. Sanesi, N. Romiti, A. Paolicchi, M. Franzini, Sensitivity and reproducibility enhancement in enzyme immunosorbent assays based on half fragment antibodies, Anal. Biochem. (2020), 114090, https://doi.org/10.1016/j.ab.2020.114090.

[17] S.L. Filbrun, A.B. Filbrun, F.L. Lovato, S.H. Oh, E.A. Driskell, J.D. Driskell, Chemical modification of antibodies enables the formation of stable antibody–gold nanoparticle conjugates for biosensing, Analyst 142 (2017) 4456–4467, https://doi.org/10.1039/C7AN01496A.

[18] T. Ibii, M. Kaieda, S. Hatakeyama, H. Shiotsuka, H. Watanabe, M. Umetsu, I. Kumagai, T. Imamura, Direct immobilization of gold-binding antibody fragments for immunosensor applications, Anal. Chem. 82 (2010) 4229–4235, https://doi.org/10.1021/ac100557k.

[19] A. Kausaite-Minkstimiene, A. Ramanaviciene, J. Kirlyte, A. Ramanavicius, Comparative study of random and oriented antibody immobilization techniques on the binding capacity of immunosensor, Anal. Chem. 82 (2010) 6401–6408, https://doi.org/10.1021/ac100468k.

[20] N. Mustafaoglu, T. Kiziltepe, B. Bilgicer, Site-specific conjugation of antibody on gold nanoparticle surface for one-step diagnosis of prostate specific antigen with dynamic light scattering, Nanoscale 9 (2017) 8684–8694, https://doi.org/10.1039/c7nr03096g.

[21] R. Varadarajan, Fortune at the bottom of the innovation pyramid: the strategic logic of incremental innovations, Bus. Horiz. 52 (2009) 21–29, https://doi.org/10.1016/j.bushor.2008.03.011.

[22] E. Candolfi, R. Ramirez, M.P. Hadju, C. Shubert, J.S. Remington, The Vitek immunodiagnostic assay for detection of immunoglobulin M toxoplasma antibodies, Clin. Diagn. Lab. Immunol. 1 (1994) 401–405, https://doi.org/10.1128/cdli.1.4.401-405.1994.

[23] J. Kimling, M. Maier, B. Okenve, V. Kotaidis, H. Ballot, A. Plech, Turkevich method for gold nanoparticle synthesis revisited, J. Phys. Chem. B 110 (2006) 15700–15707, https://doi.org/10.1021/jp061667w.

[24] C.A. Schneider, W.S. Rasband, K.W. Eliceiri, NIH Image to ImageJ: 25 years of image analysis, Nat. Methods 9 (2012) 671–675, https://doi.org/10.1038/nmeth.2089.

[25] S.W. Myint, N. Lam, A study of lacunarity-based texture analysis approaches to improve urban image classification, Comput. Environ. Urban Syst. 29 (2005) 501–523, https://doi.org/10.1016/j.compenvurbsys.2005.01.007.

[26] H. Sharma, R. Mutharasan, Half antibody fragments improve biosensor sensitivity without loss of selectivity, Anal. Chem. 85 (2013) 2472–2477, https://doi.org/10.1021/ac3035426.

[27] S.K. Vashist, J.H.T. Luong, Chapter 4 - bioanalytical requirements and regulatory guidelines for immunoassays, in: S.K. Vashist, J.H.T. Luong (Eds.), Handb. Immunoass. Technol., Academic Press, 2018, pp. 81–95, https://doi.org/10.1016/B978-0-12-811762-0.00004-9.

[28] E. Desimoni, B. Brunetti, About estimating the limit of detection by the signal to noise approach, Pharm. Anal. Acta 6 (2015) 1–4, https://doi.org/10.4172/2153-2435.1000355.

[29] ICH, Validation of Analytical Procedures: Text and Methodology, 1995, in: https://www.ema.europa.eu/en/ich-q2r2-validation-analytical-procedures-scientific-guideline.

[30] R. Mione, M. Barichello, P. Sartorello, A. Leon, P. Barioli, M. Gion, Third-generation PSA: ultrasensitive or ultraprecise assay? Int. J. Biol. Markers 10 (1995) 229–233.

[31] I.M. Thompson, R.K. Valicenti, P. Albertsen, B.J. Davis, S.L. Goldenberg, C. Hahn, E. Klein, J. Michalski, M. Roach, O. Sartor, J.S. Wolf, M.M. Faraday, Adjuvant and salvage radiotherapy after prostatectomy: AUA/ASTRO guideline, J. Urol. 190 (2013) 441–449, https://doi.org/10.1016/j.juro.2013.05.032.

[32] M.H. Black, M. Giai, R. Ponzone, P. Sismondi, H. Yu, E.P. Diamandis, Serum total and free prostate-specific antigen for breast cancer diagnosis in women, Clin. Cancer Res. Off. J. Am. Assoc. Cancer Res. 6 (2000) 467–473.

[33] D.N. Melegos, E.P. Diamandis, Is prostate-specific antigen present in female serum? Clin. Chem. 44 (1998) 691–692.

[34] E.P. Diamandis, H. Yu, D.J.A. Sutherland, Detection of prostate-specific antigen immunoreactivity in breast tumors, Breast Cancer Res. Treat. 32 (1994) 301–310, https://doi.org/10.1007/BF00666007.

[35] H. Yu, M. Giai, E.P. Diamandis, D. Katsaros, D.J. Sutherland, M.A. Levesque, R. Roagna, R. Ponzone, P. Sismondi, Prostate-specific antigen is a new favorable prognostic indicator for women with breast cancer, Cancer Res. 55 (1995) 2104–2110.

[36] H. Yu, E.P. Diamandis, D.J. Sutherland, Immunoreactive prostate-specific antigen levels in female and male breast tumors and its association with steroid hormone receptors and patient age, Clin. Biochem. 27 (1994) 75–79, https://doi.org/10.1016/0009-9120(94)90015-9.